Structure and Lithium Insertion in Oxides of Molybdenum

Rebecca C. Vincent,[1] Anthony K. Cheetham,[1] and Ram Seshadri[1]
Materials Department and Materials Research Laboratory
University of California, Santa Barbara, California 93106,
United States

(Dated: 17 December 2022)

Oxides MoO_x of molybdenum have a rich structural chemistry arising from the accommodation of oxygen deficiency as MoO_3 is reduced, and varied redox behavior arising from the ability of Mo to take on several different oxidation states. We review MoO_3, MoO_2, and all the reduced Mo oxides with intermediate compositions for their performance as Li-ion battery electrode materials. These reduced oxides are perhaps the most structurally diverse in the field of energy storage materials, taking on structures ranging from ones with crystallographic shear to bronze-like structures and distorted rutile. Crystal structure can have a significant impact on the performance of battery materials, which makes the reduced Mo oxides a promising domain of study. Electrochemical studies of these oxides from as early as 1971 to as recently as 2022 are compiled, and characteristics of capacity, capacity retention, and rate performance are compared. We find that certain oxides indeed display promising and highly reversible capacities for Li^+ storage. Typical redox voltages for Mo oxides lie in a regime that hinders maximizing energy density when they are paired with higher-voltage cathodes or lower-voltage anodes. The possibility of decreasing the redox voltage in the future will expand the promise of these materials, while offering an alternative to more critical elements such as Nb.

I. INTRODUCTION

Shear-structured materials have emerged as promising high-rate Li-ion battery electrodes, with voltages that make them suitable for use as anodes.[1–10] The vast majority of these materials are Nb-based oxides, and the research community turned to them with renewed interest following the report from Goodenough and coworkers on $TiNb_2O_7$ anodes.[1,2] These shear-phase structures are made up of transition metal octahedra (usually Nb, coordinated with 6 O).[11] Corner sharing "blocks" in the structures result in channels that promote Li^+–ion transport, and edge-sharing regions promote electronic conductivity.[12] These materials also exhibit high electrode capacity because Nb is stable at several oxidation states, allowing every Nb atom in the material to accept and release more than one electron. Furthermore, all of the oxidation states of Nb are stable in octahedral coordination environments, meaning that there are minimal structural changes during cycling, which allows for stable long term cycling.

Reduced Mo oxides with compositions between MoO_3 and MoO_2 (often referred to as "non-stoichiometric" oxides in the literature) form a wide range of structures,[13] including related shear structures, and could also be quite promising as fast-charging electrodes.[14] As demand for Nb increases, it will be important to diversify which elements can be utilized in fast cycling batteries. While Mo has been classified as having "elevated criticality" due to its economic vulnerability, Nb has "high criticality" and faces significantly more global supply risk than Mo.[15] Mo^{6+}, Mo^{5+}, Mo^{4+}, and Mo^{3+} are all readily accessible oxidation states, and multielectron redox has been observed in reduced Mo oxides between Mo^{6+} and Mo^{4+}.[14] Mo^{3+} is not present in pure Mo oxides, but has been accessed via Li insertion into battery materials.[16,17] While reducing Mo^{4+} to Mo^{3+} via Li addition is usually an unfavorable conversion reaction, insertion mechanisms have been shown in materials with very specific structural types: $LiScMo_3O_8$, which has metal-metal bonding between Mo atoms in the structure,[17] and MoO_2 whose structure contains Mo-Mo pairing.[16] These structural motifs are not present in the majority of Mo oxides between MoO_3 and MoO_2, so Mo in these materials is not expected to be reversibly cycled below an oxidation state of Mo^{4+}.

Multielectron redox behavior should enable high capacity electrodes. However when compared to Nb in Nb oxides, the higher average oxidation state on Mo in Mo oxides

results in a higher average voltage versus Li/Li^+.[14] This would lower the average cell voltage if the Mo oxide was used as an anode, and therefore lower the energy density of the cell. It is possible that the redox potential of Mo versus Li could be reduced by modifying the structure of the Mo oxide, and/or the ratio of Li and O to Mo, via the inductive effect.[18,19] The inductive effect has often been leveraged to increase the voltage of cathode materials, but less so to lower the voltage of anode materials.

The literature on Mo oxides, including structural work from the 1950s and electrochemical Li storage studies from the 1970s and 80s, has been largely piecemeal. We feel that a perspective that systematically considers structural evolution and the ability of Mo oxides to function as electrodes in Li^+–ion batteries is timely. Some mixed Mo-W oxides also form these shear structures,[20] but given the high mass of W, the focus here is on pure Mo oxides. Section II of this perspective describes the complex crystal chemistry of the Mo-O system between MoO_2 and MoO_3, while section III summarizes the electrochemical studies that have been conducted in this area.

II. STRUCTURES OF MOLYBDENUM OXIDES

Reduced Mo oxides are generally prepared *via* solid state comproportionation reactions.[14,21,22] MoO_3 powder is combined with either MoO_2 or Mo metal powder in the desired stoichiometry, pressed into a pellet, and then reacted within an evacuated and sealed silica ampoule.[22] MoO_3 can react with the silica tube, so sometimes for longer or hotter reactions the pellet is wrapped in platinum foil.[21] Reactions with the wall of the tube is known to result in lower oxygen content than desired. Early studies of the reduced Mo oxide phase space utilized larger crystals for single crystal X-ray diffraction, so at lower temperatures the reactions took weeks and included intermittent regrinding.[21] At higher temperatures, a few days were sufficient to achieve equilibrium.[21] More recent studies on polycrystalline powders, like the study of Mo_4O_{11}, achieved phase pure products after just 3 hours.[14] All reactions ended by quenching the sealed sample in water.[22]

As Mo is reduced from Mo^{6+}, a number of different crystal structures form before the oxidation state of Mo is purely Mo^{4+} as in MoO_2.[32] All the reliably reported structures that we have found are displayed in Figure 1. It is remarkable how many distinctly different crystal structure families are found in the small composition range x = 2.75 to 3.0 in

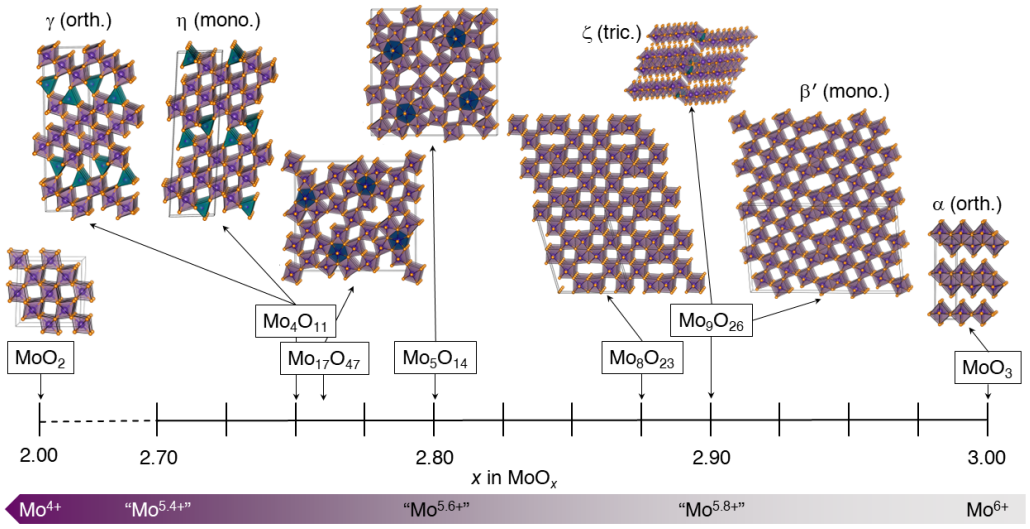

FIG. 1. Crystal structures of known compounds in the composition range from MoO_3 to MoO_2. From right to left: MoO_3,[23] shear Mo_9O_{26},[24] triclinic Mo_9O_{26},[25] Mo_8O_{23},[26] Mo_5O_{14},[27] $Mo_{17}O_{47}$,[28] monoclinic Mo_4O_{11},[29] orthorhombic Mo_4O_{11},[14] and MoO_2.[30] Unit cells of each are outlined in black. Mo atoms are within MoO_6 octahedra (represented in purple), MoO_4 tetrahedra (represented in teal), or MoO_7 pentagonal bipyramids (represented in blue). Crystal structures depicted using VESTA.[31]

MoO_x. While reduced Nb oxides all form block-type shear structures, reduced Mo oxides stably form structures belonging to 6 different structural families: layered MoO_3-type, step-lattice, Magnéli-type shear, bronze-like, Mo_4O_{11}-type with layers of both octahedra and tetrahedra, and rutile. The individual structures are discussed in some detail in the various sections of this contribution. There has been experimental evidence of additional metastable phases that are not further discussed here.[22]

The Mo-O phase diagram in the composition range $x = 1.5$ to 3.0 (in MoO_x) is displayed in Figure 2(a), redrawn from the data presented in the work of Bygdén et al.[33] MoO_2 and MoO_3 seem to be the only Mo oxides in this composition range which are stable above about 1130 K.[21,22,33] The synthesis conditions for the distinct different structures as a function of temperature and composition diagram are displayed in Figure 2(b), using data redrawn from Kihlborg.[21] Kihlborg found that equilibrium conditions were met very slowly in a number of temperature and composition regions.[22] To establish the true sta-

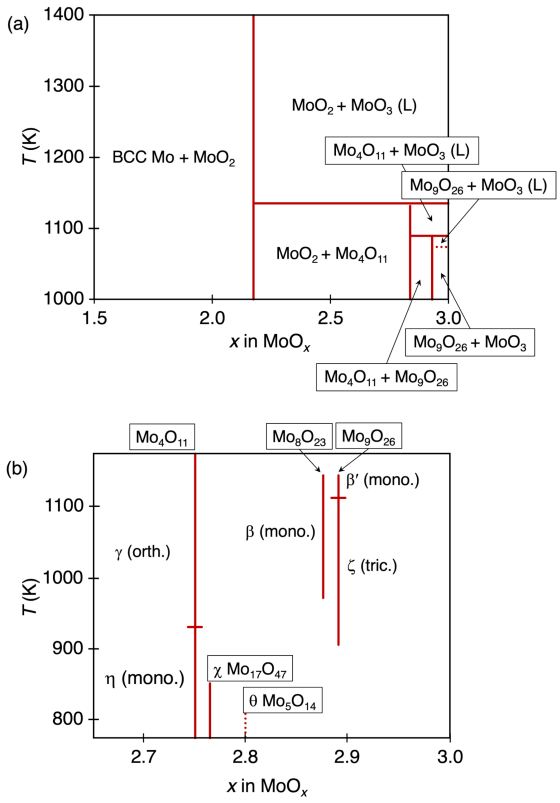

FIG. 2. (a) An enlarged section of the Mo-O phase diagram in the composition range x = 1.5 to 3.0 in MoO_x, redrawn from the work of Bygdén et al.[33] (b) Formation temperature *vs.* composition diagram for Mo oxides redrawn from the work of Kihlborg.[21]

bility regions, and therefore the basis for a real, more detailed phase diagram, would be a difficult and very time consuming task and was not attempted.[22] More details about the precise nature of the individual structures are described within the sections below.

As with Nb and W oxides, oxygen deficiency in Mo oxides is often accommodated by increasing the amount of edge-sharing between octahedral features, thus avoiding the formation of oxygen vacancies.[32,34,35] This commonly occurs as crystallographic shear,[22] for which a schematic is shown in Figure 3(a) and (b). A completely corner-connected structure like ReO_3 [Figure 3(a)] would possess an *M*:O ratio of 1:3, and a completely edge-connected structure (like rock-salt, not shown here) would possess an *M*:O ratio of 1:1. However, edge sharing in Mo is not simply determined by the metal oxygen ratio as it is in the Nb and W Wadsley-Roth systems.[13] Mo^{6+} undergoes a stronger second-order Jahn-Teller (SOJT) distortion than Nb^{5+} does, which can result in very short Mo–O bonds (equivalent to what is seen in molybdenyl ions in molecular species) which impacts

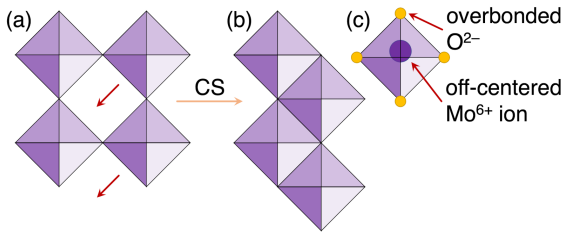

FIG. 3. (a) to (b) is a schematic of crystallographic shear (CS) in octahedrally coordinated metal oxides, resulting in octahedral features transforming from being purely corner-shareing to becoming edge-sharing. (c) A demonstration of the effect of a second order Jahn-Teller (SOJT) distortion on the position of the Mo^{6+} within an octahedra of O. One of the Mo-O covalent bonds gets shorter, increasing the positive charge density near the O and preventing that O from bonding with another Mo.

the adopted structures, since very short M–O distances result in "overbonded" oxygen atoms that remain dangling and not bonded to any other Mo.[36,37] The SOJT effect is stronger in Mo^{6+} than in Nb^{5+} which is in turn stronger than for Zr^{4+} since the driver is the charge/radius ratio.[36,37]

A. MoO_3 and MoO_2

The two most common Mo oxides are MoO_3 [Figure 4(a)] and MoO_2 [Figure 4(b)], which both form structures with Mo atoms octahedrally coordinated by O atoms. Anhydrous α-MoO_3 (space group $Pnma$) does not take the familiar cubic ReO_3 perovskite structure which is comprised of only corner-sharing octahedra extending infinitely in three dimensions. Instead, α-MoO_3 adopts an orthorhombic, layered structure made up of distorted octahedra in which each layer is edge-sharing in one direction (forming zig-zag rows) and corner-sharing in the other (along the c axis).[22,25,29]

MoO_3 does not form an ReO_3 structure because Mo^{6+} undergoes a strong SOJT distortion, as depicted in Figure 3(c). Bonds to the highly positive Mo^{6+} ion become more covalent in character rather than ionic, which shortens some of the bonds. This is able to occur because Mo^{6+} is d_0 (in comparison, Re^{6+} has 1 d electron which delocalizes in the structure) and is not repelled by the electrons on the O^{2-}. In the shortened Mo-O bonds, the positive charge density near the O is increased, causing that O to be "over-

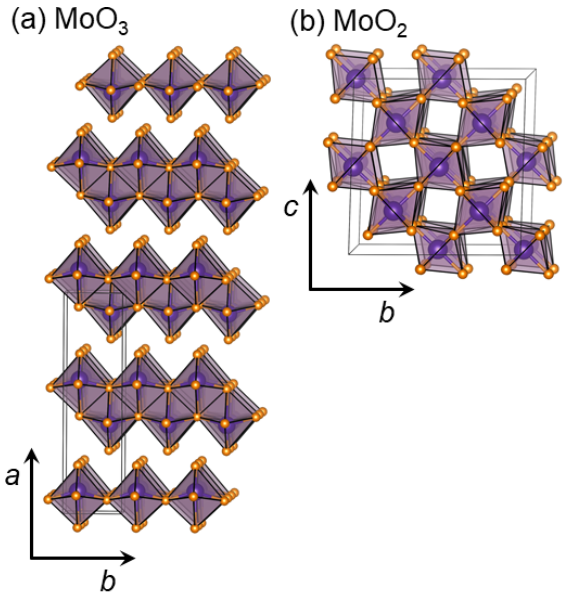

FIG. 4. (a) The structure of MoO_3[23] with the unit cell outlined in black and projected almost down the a axis. Mo^{6+} atoms sit inside octahedra of oxygen atoms. (b) The unit cell of MoO_2[30] projected almost down the c axis. Mo^{4+} atoms sit inside octahedra of oxygen atoms. Crystal structures depicted using VESTA.[31]

bonded" which prevents it from bonding with another Mo. In α-MoO_3, this causes the gaps between layers in which all the O atoms are just bonded to one Mo. It is worth noting that many reported structures of MoO_3 actually catalog the hydrated structure. Metastable β-MoO_3 takes the WO_3 structure, a highly distorted ReO_3-type (though ReO_3 is doggedly cubic, while the distortion in WO_3 makes it monoclinic).[38] Although W^{6+} is also a highly positive, d_0 ion, it experiences the SOJT effect less strongly due to increased electron shielding.

The MoO_2 (δ-Mo oxide) structure displayed in Figure 4(b) is a distorted, metal-metal bonded rutile comprising "columns" of octahedra in which there is edge sharing within each column and corner sharing between columns.

B. Mo oxide shear phases: Mo_9O_{26} and Mo_8O_{23}

Mo_8O_{23} (β-Mo oxide) and Mo_9O_{26} (β'-Mo oxide) are Magnéli phases which have shear planes similar to the block structures, but they remain structurally unique because the shear is in one direction rather than two.[39] The structures are given in Figures 5(a) and

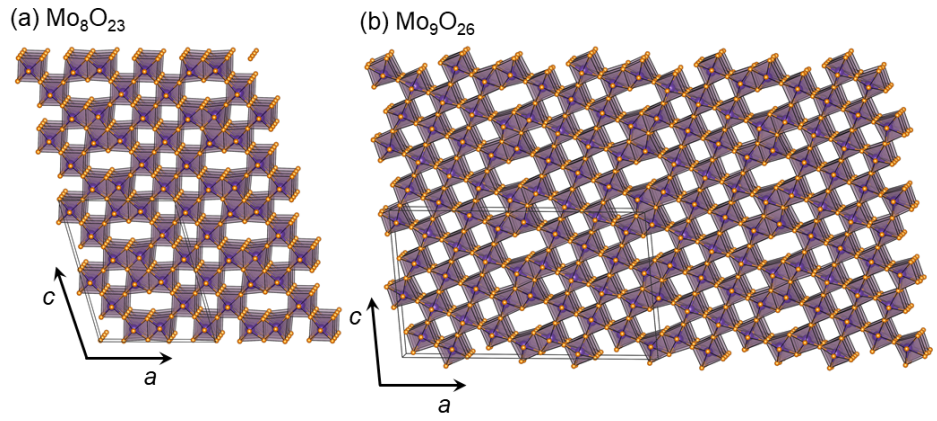

FIG. 5. (a) The structure of Mo_8O_{23}[26] with the unit cell outlined in black and projected almost down the b axis. (b) The unit cell of the shear-structured Mo_9O_{26}[24] polymorph projected almost down the b axis. Crystal structures depicted using VESTA.[31]

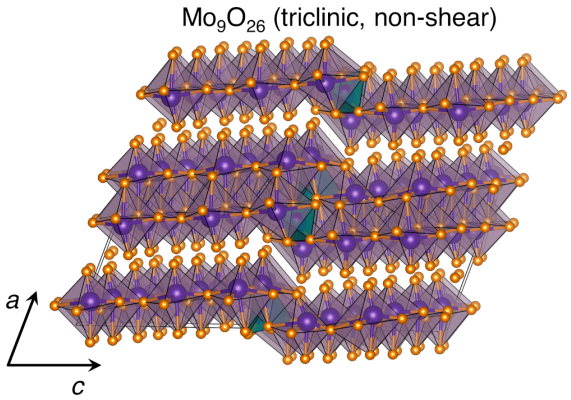

FIG. 6. The structure of triclinic, non-shear Mo_9O_{26}[25] projected almost down the b axis. Octahedrally coordinated Mo are represented in purple, while tetrahedrally coordinated Mo are represented in teal. Crystal structure depicted using VESTA.[31]

(b), respectively. In Magnéli phases, the basic ReO_3 structure extends infinitely in two dimensions, forming slabs of a finite width which are then connected with edge sharing between octahedra.[34] Previous literature classifies these compounds as being members of a homologous series of phases M_nO_{3n-3} in which $n = 8$ and $n = 9$, and n determines the characteristic thickness of the ReO_3-type slabs within the shear structure.[22,34] Mixed Mo-W oxides have been prepared which represent higher members of this series (n = 8, 9, 10, 11, 12, and 14);[20] however, the nomenclature can be confusing because lower members of this empirical formula series do not form shear structures (Mo_4O_{11} and Mo_5O_{14}).

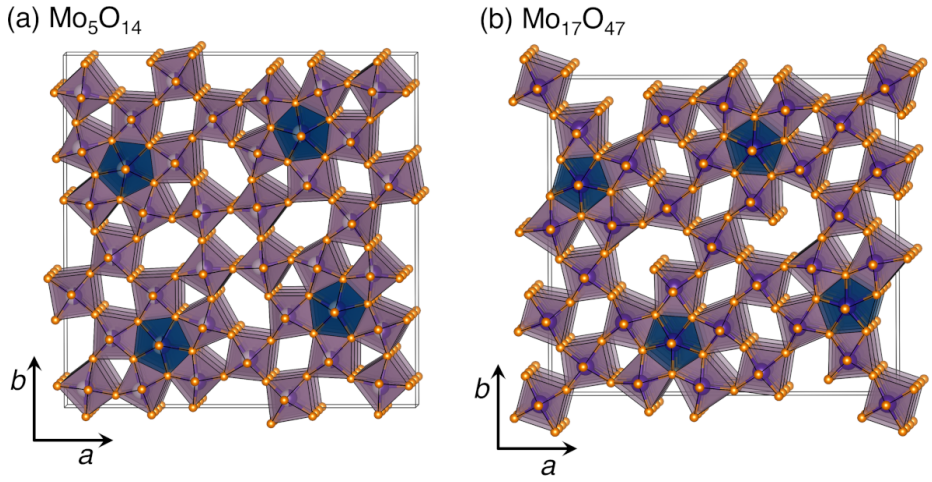

FIG. 7. (a) The tetragonal unit cell of Mo_5O_{14}[27] projected almost down the c axis. (b) The orthorhombic unit cell of $Mo_{17}O_{47}$[28] projected almost down the c axis. Mixed-oxidation Mo atoms sit inside octahedra (represented in purple) and pentagonal bipyramids (represented in blue) of oxygen atoms. Crystal structures depicted using VESTA.[31]

There is also a triclinic, non-shear polymorph of Mo_9O_{26} (ζ-Mo oxide, or ϵ in older literature[22]) which has the structure shown in Figure 6. This polymorph is often referred to as $Mo_{18}O_{52}$ in the literature to differentiate it from the shear structures in the homologous series M_nO_{3n-3}. The pseudo-layered structure is derived from α-MoO_3-type strips connected to each other by tetrahedra and edge-sharing and forming a 'step lattice.'[29] One study suggested that triclinic Mo_9O_{26} was more likely metastable and excluded it from a provisional Mo-O phase diagram.[32]

C. Pentagonal bipyramid bronze-like structures: Mo_5O_{14} and $Mo_{17}O_{47}$

Mo_5O_{14} is another oxide that fits the Mo_nO_{3n-1} pattern but does not form a Magnéli phase. It was first observed and reported as the metastable θ-Mo oxide phase in the formation temperature v. composition diagram reproduced in Figure 2(b).[21] It is reportedly difficult to prepare reproducibly,[27,40–42] and very susceptible to the formation of twinning defects.[40,43] The phase can be stabilized by partially substituting Mo with group 4 or 5 elements, which decreases the number of non-bonding valence electrons.[40,44] $Mo_{17}O_{47}$ has a similar structure to Mo_5O_{14},[27] though it is more stable and therefore can be made as a single phase in the form of thin, fragile needles.[45]

Both Mo_5O_{14} and $Mo_{17}O_{47}$ (χ-Mo oxide) form complicated arrays of polyhedra in 2D, containing distorted MoO_7 pentagonal bipyramids which share their 5 equatorial edges with distorted MoO_6 octahedra,[44] as well as three- to six-membered rings.[27] These complicated 2D polygonal networks are then corner-connected in the third dimension, perpendicular to the rings, forming large, open channels.[27] The two structures are regarded as belonging to a common structural family with $W_{18}O_{49}$.[27,45] Mo_5O_{14} is slightly less dense (oxygen atoms per volume) than $Mo_{17}O_{47}$ and $W_{18}O_{49}$, which could be related to its metastability.[27] The structures of Mo_5O_{14} and $Mo_{17}O_{47}$ are shown in Figures 7(a) and (b), respectively,[45] and are projected looking down the channels. Both have been referred to as 'tunnel structures'[43] that are closely related to the tetragonal and hexagonal tungsten bronzes.[27] According to Wadsley, however, $Mo_{17}O_{47}$ cannot be described as a tunnel compound because its six-membered rings have one singly-bonded oxygen in the middle, thus blocking the tunnels.[27,45,46]

D. Orthorhombic and Monoclinic Mo_4O_{11}

Mo_4O_{11} also fits the Mo_nO_{3n-1} pattern but does not form a Magnéli phase. Instead it forms two polymorphs: one is the orthorhombic γ-Mo oxide depicted in Figure 8(a), and the other is the monoclinic η-Mo oxide (γ'-Mo oxide in older literature[22]), depicted in Figure 8(b), formed at lower temperatures.[29] Notably, these two structures have the lowest density of all the other stable Mo oxides as measured by oxygen atoms per volume.[22] Similar to the Magnéli phases, both structures contain two dimensional ReO_3-structured slabs made up of distorted octahedra; however, instead of being connected with edge sharing as a shear structure would be, the slabs are corner-connected with MoO_4 tetrahedra.[29] We note that tetrahedral coordination of Mo^{6+} is not unusual as it is found in many other important materials such as $Fe_2(MoO_4)_3$.[47]In the monoclinic Mo_4O_{11} structure, adjacent slabs have parallel rows and form six-membered rings with the tetrahedra, while in the orthorhombic Mo_4O_{11} structure adjacent slabs are tilted with respect to each other and form five-membered rings with the tetrahedra.[29,48] The energy difference between the two polymorphs has been hypothesized to be small,[29] but the ease of transition from one phase to the other may depend on the degree of crystalline perfection in the sample.[22] Experimentally, orthorhombic Mo_4O_{11} has been found to be the most stable reduced Mo

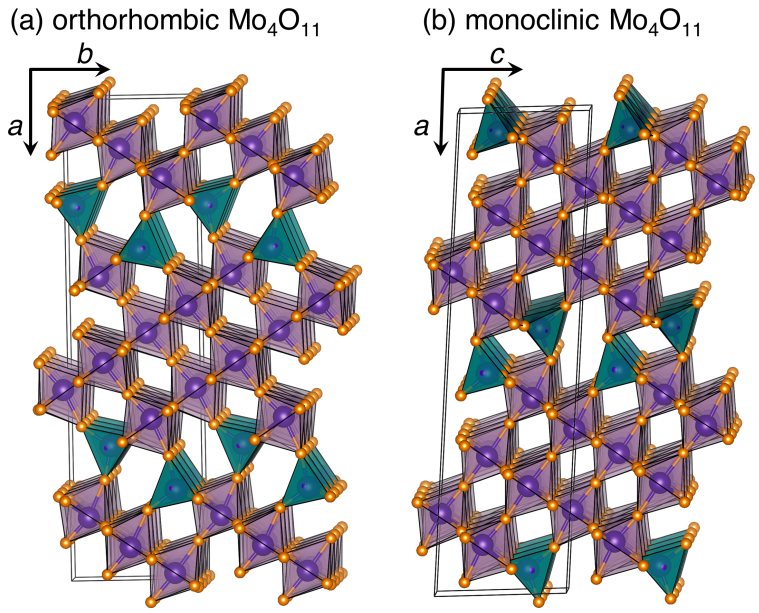

FIG. 8. (a) The unit cell of orthorhombic Mo_4O_{11} projected almost down the c axis, structure from refinement of synchrotron data reported in a previous publication about Mo_4O_{11}.[14] (b) The unit cell of monoclinic Mo_4O_{11}[29] projected almost down the b axis. Mixed-oxidation Mo atoms sit inside octahedra (represented in purple) and tetrahedra (represented in teal) of oxygen atoms. Crystal structures depicted using VESTA.[31]

oxide, and is therefore the easiest to synthesize.[14,49]

III. PREVIOUS ELECTROCHEMISTRY STUDIES OF MOLYBDENUM OXIDES

MoO_2 and MoO_3 have both been investigated as Li-ion battery electrodes. MoO_2 has good bulk electrical conductivity due to Mo-Mo pairing and electron delocalization along Mo atom chains.[50] Unfortunately, MoO_2 still shows poor rate performance perhaps due to sluggish Li diffusion kinetics[16,51,52] after the monoclinic structure, which contains ion diffusion tunnels, transforms into a badly conducting orthorhombic structure and back at 1.6 V during each charge and discharge.[50,51] The phase transition is suppressed in nanostructured MoO_2, which, along with the shorter ionic diffusion distance, allows for improved rate performance.[50] MoO_2 has most commonly been investigated as a conversion anode, in which case 4 Li are inserted per formula unit, Mo^{4+} is reduced to Mo metal, and Li_2O is formed.[50,52–54] Conversion-type electrodes are usually not useful for fast cycling or long

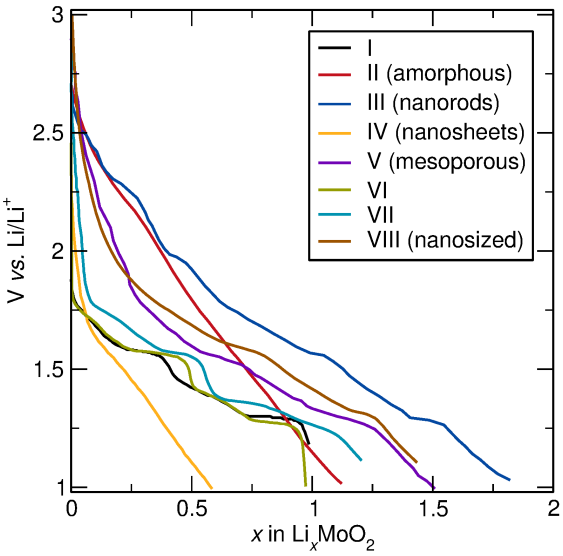

FIG. 9. Initial discharge curves of MoO_2 from seven different studies: I - Cycling of pure, ball milled material at $C/40$ calculated for 1 Li inserted per formula unit.[16] II - Cycling of amorphous MoO_2 as a pellet electrode with 70% by mass active material, 25% carbon, and 5% PTFE.[56] III - Cycling of graphitized carbon composite nanorods with electrodes composed of 60% MoO_2 by mass, 30% carbon, and 10% PVDF binder at a rate of $C/10$ calculated for 4 Li inserted per formula unit.[53] IV - Cycling of MoO_2 tremella-like nanosheets in slurry cast electrodes consisting of 80% active material, 10% carbon, and 10% PVDF.[54] V - Cycling of mesoporous MoO_2 in slurry cast electrodes consisting of 80% active material, 10% carbon, and 10% PVDF at a rate of $C/20$ calculated for 4 Li inserted per formula unit.[52] VI - Cycling of 90% MoO_2, 5% carbon fibers, and 5% PVDF by mass.[57] VII - Cycling of pure thin films of first microsized MoO_2 and then nanosized (VIII) MoO_2 at a rate of $C/10$ calculated for 1 Li inserted per formula unit.[50]

term capacity retention.[50] To investigate only the insertion-type reaction, cycling of MoO_2 must stay above a potential of 1 V vs Li/Li^+.[50] Another reason to stay above 1 V is that when using carbon composite electrodes like those used to test MoO_2 in most previous studies, much of the low voltage capacity can be attributed to the carbon itself.[55]

Figure 9 compares the discharge curves of MoO_2 reproduced from seven different published works. When the cycling was performed below 1 V, lower voltage data points were omitted in this perspective. Crystalline, microsized MoO_2 displays clearer steps in the voltage profiles, with the step first step at 1.6 V corresponding to a phase transformation from a monoclinic structure to an orthorhombic structure, and the second step at 1.3 V corre-

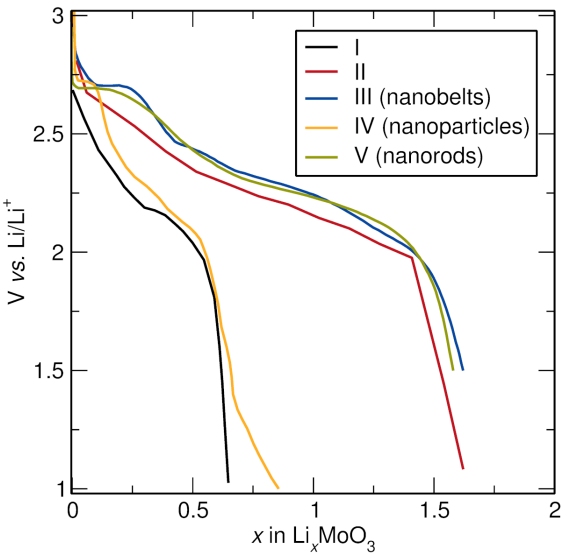

FIG. 10. Initial discharge curves of MoO_3 from five different studies: I - Cycling of a 70% MoO_3 and 30% graphite electrode.[59] II - Cycling of a 85% MoO_3, 10% graphite, and 5% polyethylene binder electrode.[60] III - Cycling of MoO_3 nanobelts in a pellet electrode with about 55% active material, 39% acetylene black, and 6% PTFE.[61] IV - Cycling of MoO_3 nanoparticles with seemingly no carbon or binder additives.[62] V - Cycling a cast electrode comprised of 70% MoO_3 nanorods, 20% carbon black, and 10% PVDF.[63]

sponding to a phase transformation back to a monoclinic structure.[50,51] The features are almost entirely smoothed out in the discharge curves of the nanosized and/or amorphous MoO_2.[50,52–54,56] Experiments that stayed above 1 V during galvanostatic cycling of MoO_2 achieved a reversible capacity of about 220 mAh g^{-1}, corresponding to the reduction of Mo^{4+} to Mo^{3+}.[50,56,57] In another study, various lithiated MoO_2 phases were prepared and then charged first, and $LiMoO_2$ achieved a capacity of 200 mAh g^{-1} when cycled between 2 V and 3.6 V.[58] However, these studies, which used a higher voltage window and thus avoided the conversion reaction voltage and the voltage at which the carbon in the electrode itself stores Li, still demonstrated detrimental capacity fade over time. This capacity fade could be due to MoO_2 dissolution into the carbonate-based electrolyte[57] which is used in most commercial Li-ion batteries.

MoO_3 is a band insulator and therefore has lower conductivity than MoO_2,[64,65] but electrochemical cycling is possible following the addition of graphite to the electrode.[59,60] Figure 10 compares the discharge curves of α-MoO_3 reproduced from five different pub-

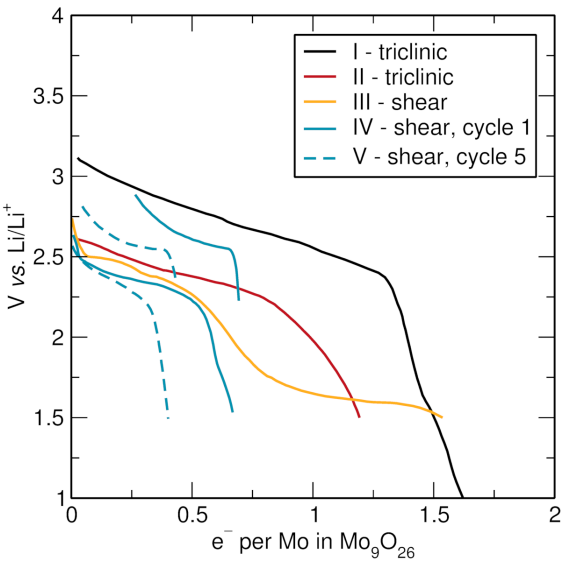

FIG. 11. Slow-rate discharge curves of Mo_9O_{26} from four different studies which used cathodes made from pressed pellets of the pure active material (without the use of conductive additives or binders). The use of pellet electrodes meant that the active material loading was high: about 13-30 mg cm^{-2}.[42,69,70] I - Triclinic Mo_9O_{26}.[71] II - Triclinic Mo_9O_{26}.[69] III - Shear-structured Mo_9O_{26}.[41] IV and V - Shear-structured Mo_9O_{26}, cycles 1 and 5 respectively of the same cell.[42]

lished works. Again, the data was not reproduced when it was recorded below 1 V so that just the insertion mechanism, not conversion, is studied. The rate performance and other electrochemical properties were significantly improved when MoO_3 took the form of nanorods and nanobelts.[61–63,66] However, capacity fade was still significant.[61,63] Nanosized α-MoO_3[67] and nanosized MoO_{3-x}[68] have also been demonstrated as pseudocapacitors, which combine bulk redox and surface charge storage for high-rate energy storage. However, nanosizing the active material is often costly on an industrial scale, so materials with greater intrinsic conductivity are still needed for commercial high-rate batteries.

Reduced Mo oxides between MoO_2 and MoO_3 may offer the desired increase in conductivity of Mo oxide active materials. Despite having a related structure to MoO_3, the conductivity of the triclinic phase of Mo_9O_{26} was measured to be orders of magnitude higher than MoO_3.[69] Relatedly, the voltage polarization of triclinic Mo_9O_{26} observed during a cyclic voltammetry experiment was lower than that of MoO_3.[69] The recharge efficiency was also demonstrated to be higher for triclinic Mo_9O_{26} than for MoO_3, though there was still some kinetic hindrance to reoxidizing, perhaps due to small structural changes asso-

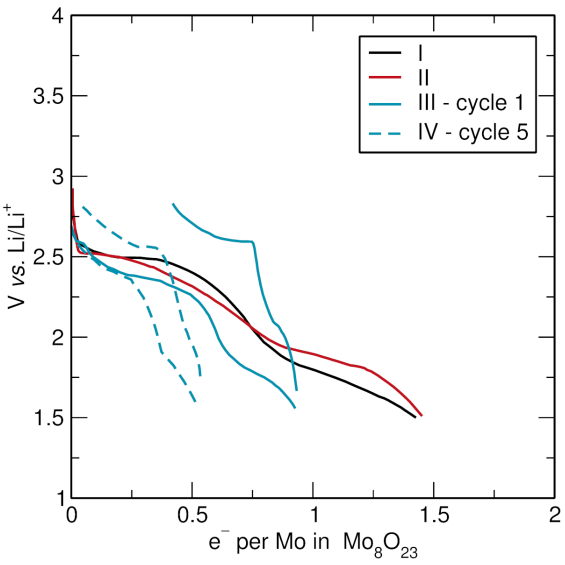

FIG. 12. Slow-rate discharge curves of Mo_8O_{23} from three different studies which used cathodes made from pressed pellets of the pure active material (without the use of conductive additives or binders). The use of pellet electrodes meant that the active material loading was high: about 13-30 mg cm^{-2}.[42,69,70] I,[41] and II.[70] III and IV are cycles 1 and 5 respectively of the same cell.[42]

ciated with Li insertion.[69] Figure 11 shows discharge curves reported in early literature in which triclinic Mo_9O_{26} demonstrated a yield of about 1.25 to 1.5 electrons per Mo atom at slow rates, indicating multielectron redox reactions which provide the potential for high capacity.[69,71] Multielectron redox of about 1.5 electrons per Mo was also demonstrated in slowly discharging batteries with electrodes made from pure shear Mo_9O_{26}[41] and Mo_8O_{23}[41,70] with a voltage cutoff of 1.5 V (see Figure 11 and Figure 12). Only one study demonstrated more than one electrochemical cycle, so cycles 1 and 5 are reproduced here even though the overall capacities achieved were lower.[42]

Mo_8O_{23}, shear-structured Mo_9O_{26}, and Mo_4O_{11} were all found to change irreversibly past a certain threshold of Li insertion,[14,72] which was hypothesized to negatively impact their recharge efficiencies.[72] However, when limited to cycling above 2 V, Mo_8O_{23} showed the best recharge efficiency (on the first cycle) of the three compounds, and performed significantly better than MoO_3, which the authors attributed to "the parallel channels of Mo_8O_{23} allow[ing] easy uptake and release of Li."[72] However, the use of a voltage cutoff of 2 V limited the total capacity to 0.89 electrons per Mo atom, and therefore did not take advantage of multielectron redox on the Mo.[70] Cyclic voltammetry curves also showed

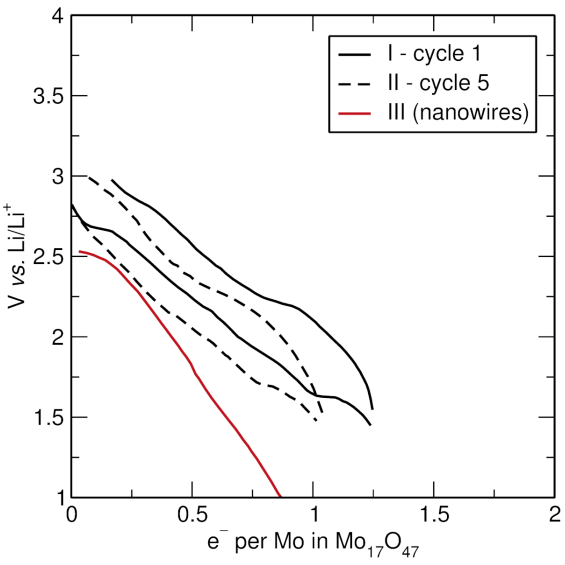

FIG. 13. I and II - Cycle 1 and 5 respectively of the same cell: slow-rate cycling of $Mo_{17}O_{47}$ using cathodes made from pressed pellets of the pure active material (without the use of conductive additives or binders) which gave an active material mass loading of around 13-25 mg cm^{-2}.[42] III - Slow-rate discharge of $Mo_{17}O_{47}$ nanowires which were grown on stainless steel substrates and directly used as the cathode in a battery.[73]

that the redox reaction was more reversible in Mo_8O_{23} than in MoO_3 or triclinic Mo_9O_{26}.[70]

Another study attempted reversible cycling of reduced Mo oxides using 1.5 V as the lower voltage cutoff, and in this voltage window found that $Mo_{17}O_{47}$ (see Figure 13) closely followed by Mo_4O_{11} (see Figure 14) had the highest reversible capacities compared to Mo_8O_{23} and shear/Magnéli-type Mo_9O_{26}.[42] Earlier studies only investigated the recharge efficiency between the first discharge and charge, which is not always a good indication of how reversible further cycling will be.[42] After 1 full cycle, 0.67 and 0.90 Li per Mo were reversibly inserted and extracted from shear/Magnéli-type Mo_9O_{26} and Mo_8O_{23}, respectively, consistent with earlier studies.[42,70] However, after 20 cycles only 0.35 and 0.29 Li/Mo, respectively, could be reversibly inserted.[42] Mo_4O_{11} and $Mo_{17}O_{47}$ fared somewhat better, fading from 1.35 to 0.77 and from 1.23 to 1.02 Li/Mo in capacity, respectively, between cycle 1 and cycle 20.[42] $Mo_{17}O_{47}$ nanowires were later synthesized, but did not demonstrate improved electrochemical properties.[73] A higher total capacity was reached, but only at much lower voltages where a conversion reaction occurred.[73]

The most recent electrochemical studies of phase-pure reduced Mo oxides have been on

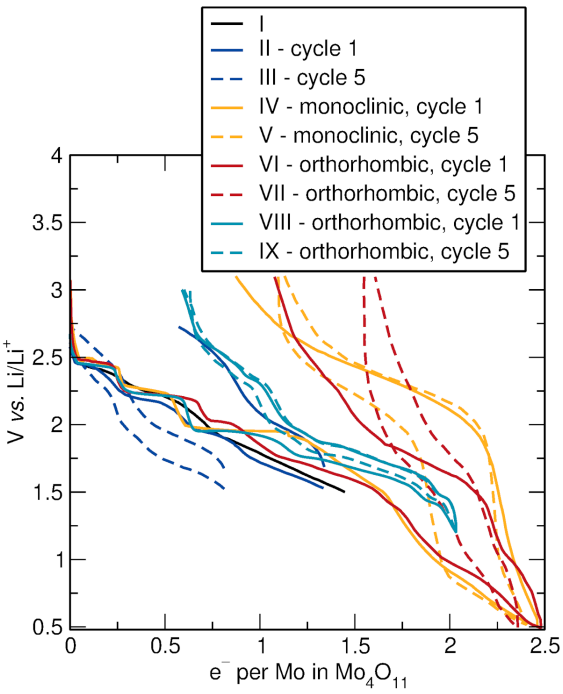

FIG. 14. Galvanostatic cycling curves of Mo_4O_{11}. I - Slow discharge of a battery using a pressed pellet cathode of pure Mo_4O_{11} (no carbon additives or binders were used).[41] II and III - Cycle 1 and 5 respectively of the same cell slowly cycling using a pressed pellet cathode of pure Mo_4O_{11} (no carbon additives or binders were used).[42] IV and V - Cycle 1 and 5 respectively of the same cell which used pressed pellet electrodes made from 89% monoclinic Mo_4O_{11}, 10% carbon black, and 1% polymer binder and was cycled slowly at a rate of approximately $C/42$.[74] VI and VII - Cycle 1 and 5 respectively of the same cell which used pressed pellet electrodes made from 89% orthorhombic Mo_4O_{11}, 10% carbon black, and 1% polymer binder and was cycled slowly at a rate of approximately $C/42$.[74] VIII and IX - Cycle 1 and 5 respectively of the same cell which used slurry cast electrodes made from 80% orthorhombic Mo_4O_{11}, 10% carbon black, and 10% PVDF; therefore the mass loading was much lower, but the cells were also cycled faster at a rate of $C/10$.[14]

Mo_4O_{11}. One study compared the properties of the orthorhombic and monoclinic phases of Mo_4O_{11}.[74] The two structures exhibited similar capacities on discharge, but with a slightly different discharge curve shape and different insertion mechanisms.[74] Mo_4O_{11} demonstrated the highest capacity of any Mo oxide thus far, exceeding the theoretical capacity on the first discharge which corresponds to reducing each Mo^{6+} and Mo^{5+} to a Mo^{4+} oxidation state (1.5 Li inserted per Mo).[14,74] (This is even more apparent in Figure 15)

When cycling with a lower voltage cutoff of 0.5 V, the monoclinic phase appeared more reversible than the orthorhombic phase after seven cycles.[74] However, composite electrodes containing 10% carbon black by mass were used to perform this electrochemistry,[74] and carbon itself stores Li at these low voltages.[55] It is hard to deconvolute the effects of carbon from the performance of the active material, which adds uncertainty to these results. More recent cycling shows very reversible cycling of orthorhombic Mo_4O_{11} between 1.2 V and 3.0 V (90% capacity retention after 100 cycles at a fast rate of $1C$).[14] The improved reversibility could be due to a more optimized voltage window. The study also showed the lowest voltage polarization in cycling of Mo_4O_{11} which could indicate an improved cell construction as well.[14] Most Mo oxides have not been cycled at varied rates; however, micrometer-scale particles of orthorhombic Mo_4O_{11} has demonstrated excellent rate performance, achieving a stable capacity of over 200 mAh g^{-1} at a $5C$ rate. *Operando* XRD measurements revealed that the structure of Mo_4O_{11} dramatically changed during the first lithiation, so the subsequent reversible cycling and good rate performance occurred in a new structure which is likely more layered than the original.[14] Some earlier studies also reported the observation of a phase change on the first discharge/lithiation of the material.[41,74] One study presented *in situ* XRD data that they interpreted as the structure becoming more amorphous with cycling (most peaks disappear).[74] However, the crystalline structure of the newly formed phase is apparent in the *operando* XRD study.[14]

Figure 15 summarizes schematic, characteristic voltage curves from four different classes of Mo oxide phases, obtained during lithiation. As anticipated, lower average starting oxidation states of Mo in the structure result in lower average redox voltages. Of the materials we have founds reports of, both polymorphs of Mo_4O_{11} demonstrate the highest capacity in their initial discharge.

IV. CONCLUSIONS

Reduced Mo oxides belong to a remarkable number of structural families in the composition range between MoO_3 and MoO_2. Despite the similarity of Mo to its periodic table neighbor Nb, their oxides form quite different structures, with Mo oxides forming a greater variety. This is, in part, because Nb is most stable being octahedrally coordinated at all oxidation states, whereas Mo is a little more flexible. Some reduced Mo oxides, like

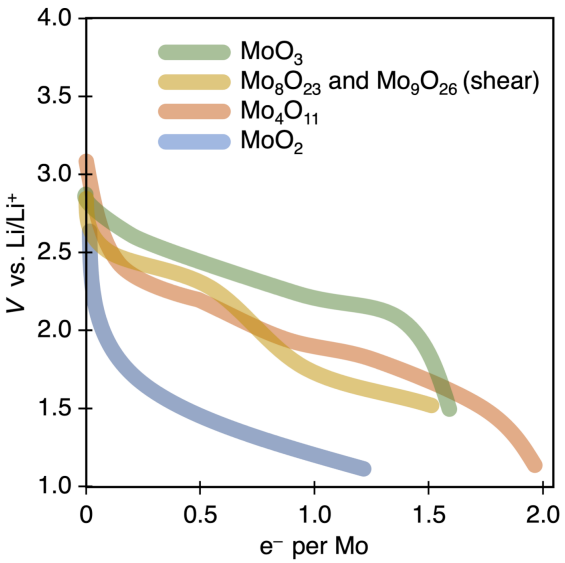

FIG. 15. Schematic characteristic galvanostatic cycling curves for four different classes of Mo oxides.

Mo_8O_{23} and the shear polymorph of Mo_9O_{26}, share structural qualities with the Nb-based Wadsley-Roth shear structures: they contain octahedrally coordinated metals with some regions of just corner-sharing, and some regions of edge-sharing. These similarities make reduced Mo oxides interesting for the purpose of fast-cycling Li-ion battery electrodes.

While reduced Mo oxides provide many diverse structures to study, they are less structurally stable with cycling than Nb oxides. However, structural change is not always a bad thing. Mo_4O_{11}, and potentially some of the other compositions, experience structure change on the first discharge/lithiation that is then stable for long term cycling and at high rates. Mo_4O_{11} also shows the highest capacity on the first discharge compared to all the other Mo oxides, and following the favorable structure change it shows the best capacity retention over time, and the best rate performance. The studies that investigated Mo_4O_{11} and demonstrated high capacities were also the most recent. Some of the success could be attributed to more modern cell designs and better optimized voltage windows for reversible cycling. This could be a compelling reason to continue the study of reduced Mo oxide electrodes – there is still much we do not know.

For each Mo oxide compound, a significant variability was found between the electrochemistry results in different studies (see Figures 9–14). The difficulty of making high quality samples of the individual Mo oxide phases could lead to such a spread in mea-

sured capacity. The authors can confirm, for example, that isolation of Mo_8O_{23} and either polymorph of Mo_9O_{26} has proven difficult. Another reason that more recent studies demonstrated the best electrochemistry results could be an improved ability to characterize sample quality and phase purity.

The unfavorable operating voltage of reduced Mo oxides makes them awkward for use as either cathodes or anodes. This will prevent them from overtaking the total energy storage performance of the Nb-based Wadsley-Roth shear structures, even if the gravimetric capacities are comparable. However, when working with rare elements, variety is needed. Mo is even classified as less "critical" than Nb because of its lower global supply risk.[15] Future work could also be dedicated to decreasing the redox potential of reduced Mo oxides to make a more effective Li-ion battery anode.[17]

ACKNOWLEDGMENTS

RCV acknowledges the National Science Foundation for a Graduate Research Fellowship (NSF DGE-2139319). This work was supported as part of the Center for Synthetic Control Across Length-scales for Advancing Rechargeables (SCALAR), United States, an Energy Frontier Research Center funded by the U.S. Department of Energy, Office of Science, Basic Energy Sciences under DE-SC0019381.

REFERENCES

[1]J.-T. Han, Y.-H. Huang, and J. B. Goodenough, "New anode framework for rechargeable lithium batteries," Chem. Mater. **23**, 2027–2029 (2011).

[2]J.-T. Han and J. B. Goodenough, "3-V full cell performance of anode framework $TiNb_2O_7$/spinel $LiNi_{0.5}Mn_{1.5}O_4$," Chem. Mater. **23**, 3404–3407 (2011).

[3]K. J. Griffith, A. Senyshyn, and C. P. Grey, "Structural stability from crystallographic shear in TiO_2-Nb_2O_5 phases: Cation ordering and lithiation behavior of $TiNb_{24}O_{62}$," Inorg. Chem. **56**, 4002–4010 (2017).

[4]K. J. Griffith, K. M. Wiaderek, G. Cibin, L. E. Marabella, and C. P. Grey, "Niobium tungsten oxides for high-rate lithium-ion energy storage," Nature **559**, 556–563 (2018).

[5]K. J. Griffith, K. M. Wiaderek, G. Cibin, L. E. Marbella, and C. P. Grey, "Niobium tungsten oxides for high-rate lithium-ion energy storage," Nature **559**, 556–563 (2018).

[6]M. B. Preefer, M. Saber, Q. Wei, N. H. Bashian, J. D. Bocarsly, W. Zhang, G. Lee, J. Milam-Guerrero, E. S. Howard, R. C. Vincent, B. C. Melot, A. Van der Ven, R. Seshadri, and B. S. Dunn, "Multielectron redox and insulator-to-metal transition upon lithium insertion in the fast-charging, wadsley-roth phase PNb_9O_{25}," Chem. Mater. **32**, 4553–4563 (2020).

[7]K. J. Griffith and C. P. Grey, "Superionic lithium intercalation through 2×2 nm^2 columns in the crystallographic shear phase $Nb_{18}W_8O_{69}$," Chem. Mater. **32**, 3860–3868 (2020).

[8]K. E. Wyckoff, D. D. Robertson, M. B. Preefer, S. M. L. Teicher, J. Bienz, L. Kautzsch, T. E. Mates, J. A. Cooley, S. H. Tolbert, and R. Seshadri, "High-capacity Li^+ storage through multielectron redox in the fast-charging wadsley-roth phase $W_{0.2}V_{0.8})_3O_7$," Chem. Mater. **32**, 9415–9424 (2020).

[9]K. McColl, K. J. Griffith, R. L. Dally, R. Li, J. E. Douglas, K. R. Poeppelmeier, F. Cora, I. Levin, and M. M. Butala, "Energy storage mechanisms in vacancy-ordered wadsley-roth layered niobates," J. Mater. Chem. A **9**, 20006–20023 (2021).

[10]K. J. Griffith, Y. Harada, R. M. R. S. Egusa, R. S. Monteiro, R. B. V. Dreele, A. K. Cheetham, R. J. Cava, C. P. Grey, , and J. B. Goodenough, "Titanium niobium oxide: From discovery to application in fast-charging lithium-ion batteries," Chem. Mater. **33**, 4–18 (2021).

[11]B. G. Hyde, A. N. Bagshaw, S. Andersson, and M. O'Keeffe, "Some defect structures in crystalline solids," Annu. Rev. Mater. Sci. **4**, 43–92 (1974).

[12]J. Gopalakrishnan, "Insertion/extraction of lithium and sodium in transition metal oxides and chalcogenides," Bull. Mater. Sci. **7**, 201–214 (1985).

[13]A. A. Voskanyan and A. Navrotsky, "Shear pleasure: The structure, formation, and thermodynamics of crystallographic shear phases," Annu. Rev. Mater. Res. **51**, 521–540 (2021).

[14]R. C. Vincent, Y. Luo, J. L. Andrews, A. Zohar, Y. Zhou, Q. Yan, E. M. Mozur, M. B. Preefer, J. Nelson Weker, A. K. Cheetham, J. Luo, L. Pilon, B. C. Melot, B. Dunn, and R. Seshadri, "High-rate lithium cycling and structure evolution in Mo_4O_{11}," Chem. Mater. **34**, 4122–4133 (2022).

[15]P. A. J. Lusty, R. A. Shaw, A. G. Gunn, and I. N. E., "UK criticality assessment of technology critical minerals and metals." Tech. Rep. CR/21/120 (British Geological Survey,

Keyworth, Nottingham, 2021).

[16]J. R. Dahn and W. R. McKinnon, "Structure and electrochemistry of Li_xMoO_2," Solid State Ion. **23**, 1–7 (1987).

[17]K. E. Wyckoff, J. L. Kaufman, S. W. Baek, C. Dolle, J. J. Zak, J. Bienz, L. Kautzsch, R. C. Vincent, A. Zohar, K. A. See, Y. M. Eggeler, L. Pilon, A. V. der Ven, and R. Seshadri, "Metal–metal bonding as an electrode design principle in the low-strain cluster compound $LiScMo_3O_8$," J. Am. Chem. Soc. **144**, 5841–5854 (2022).

[18]A. K. Padhi, K. S. Nanjundaswamy, C. Masquelier, S. Okada, and J. B. Goodenough, "Effect of structure on the Fe^{3+}/Fe^{2+} redox couple in iron phosphates," J. Electrochem. Soc. **144**, 1609–1613 (1997).

[19]B. C. Melot, D. O. Scanlon, M. Reynaud, G. Rousse, J.-N. Chotard, M. Henry, , and J.-M. Tarascon, "Chemical and structural indicators for large redox potentials in Fe-based positive electrode materials," ACS Appl. Mater. Interfaces **6**, 10832–10839 (2014).

[20]A. Magnéli, B. Blomberg-Hansson, L. Kihlborg, and G. Sundkvist, "Studies on molybdenum and molybdenum wolfram oxides of the homologous series Me_nO_{3n-1}," Acta Chem. Scand. **9**, 1382 (1955).

[21]L. Kihlborg, "Studies on molybdenum oxides," Acta Chem. Scand. **13**, 954–962 (1959).

[22]L. Kihlborg, "The structural chemistry of the higher molybdenum oxides," Arkiv f or Kemi **21**, 471–495 (1963).

[23]H. Negishi, S. Negishi, Y. Kuroiwa, N. Sato, and S. Aoyagi, "Anisotropic thermal expansion of layered MoO_3 crystals," Phys. Rev. B **69**, 109902 (2004).

[24]M. Sato, M. Onoda, and Y. Matsuda, "Structural transitions in $Mo_nO_{3n-1}(n =$9 and 10)," J. Phys. C: Solid State Phys. **20**, 4763–4771 (1987).

[25]L. Kihlborg, "The crystal structure of $Mo_{18}O_{52}$ and the existence of homologous series of structures based on MoO_3," Arkiv f or Kemi **21**, 443–460 (1963).

[26]A. J. H. Komdeur, J. L. de Boer, and S. van Smaalen, "Determination of the incommensurately modulated structure of Mo_8O_{23} by means of single-crystal X-ray diffraction," J. Phys. Condens. Matter **2**, 45–54 (1990).

[27]L. Kihlborg, "Crystal structure studies on Mo_5O_{14}, a compound exhibiting two-dimensional disorder," Arkiv f or Kemi **21**, 427–437 (1963).

[28]N. Yamazoe, T. Ekström, and L. Kihlborg, "Structural effects of vanadium substitution in $Mo_{17}O_{47}$," Acta Chem. Scand. **29**, 404–408 (1975).

[29]L. Kihlborg, "Crystal structure studies on monoclinic and orthorhombic Mo_4O_{11}," Arkiv f or Kemi **21**, 365–377 (1963).

[30]B. G. Brandt, "On the crystal structures of MoO_2 and $MoO_3(H_2O)_2$. an account of computer programming and structure refinement," Chem. Comm. , 1–41 (1971).

[31]K. Momma and F. Izumi, "VESTA: a three-dimensional visualization system for electronic and structural analysis," J. Appl. Crystallogr. **41**, 653–658 (2008).

[32]L. Brewer and R. H. Lamoreaux, "The Mo-O system (molybdenum-oxygen)," Bull. Alloy Phase Diagr. **1**, 85–89 (1980).

[33]J. Bygdén, D. Sichen, and S. Seetharaman, "A thermodynamic study of the molybdenum-oxygen system," Metall. Mater. Trans. B **25B**, 885–891 (1994).

[34]L. Kihlborg, "The crystal chemistry of molybdenum oxides," Adv. Chem. Ser. **39**, 37–45 (1963).

[35]E. Brocławik and J. Haber, "SCF-SW-Xα calculations of the removal of oxygen from oxide surfaces by vacancy formation and crystallographic shear mechanisms," J. Catal. **72**, 379–382 (1981).

[36]I. B. Bersuker, "Pseudo-jahn–teller effect—a two-state paradigm in formation, deformation, and transformation of molecular systems and solids," Chem. Rev. **113**, 1351–1390 (2013).

[37]K. M. Ok, P. S. Halasyamani, D. Casanova, M. Llunell, P. Alemany, and S. Alvarez, "Distortions in octahedrally coordinated d^0 transition metal oxides: A continuous symmetry measures approach," Chem. Mater. **18**, 3176–3183 (2006).

[38]T. Vogt, P. M. Woodward, and B. A. Hunter, "The high-temperature phases of WO_3," J. Solid State Chem. **144**, 209–215 (1999).

[39]A. Magnéli, "The crystal structures of Mo_9O_{26} (β'-molybdenum oxide) and Mo_8O_{23} (β-molybdenum oxide)," Acta Chem. Scand. **2**, 501–517 (1948).

[40]L. Kihlborg, "Stabilization of the tunnel structure of Mo_5O_{14} by partial metal atom substitution," Acta Chem. Scand. **23**, 1834–1835 (1969).

[41]P. Cignini, M. Icovi, S. Panero, G. Pistoia, and C. Temperoni, "Non-stoichiometric molybdenum oxides as cathodes for lithium cells: Part I. primary batteries," J. Electroanal. Chem. **102**, 333–341 (1979).

[42]P. A. Christian, J. N. Carides, F. J. DiSalvo, and J. V. Waszczak, "Molybdenum oxide cathodes in secondary lithium cells," J. Electrochem. Soc. **127**, 2315–2319 (1980).

[43]N. Yamazoe and L. Kihlborg, "Mo_5O_{14} - twinning and three-dimensional structure, determined from a partly tantalum-substituded crystal," Acta Cryst. **B31**, 1666 (1975).

[44]T. Ekström, "Formation of ternary phases of Mo_5O_{14} and $Mo_{17}O_{47}$ structure in the molybdenum-wolfram-oxygen system," Mater. Res. Bull. **7**, 19–26 (1972).

[45]L. Kihlborg, "The crystal structure of $Mo_{17}O_{47}$," Acta Chem. Scand. **14**, 1612–1622 (1960).

[46]A. D. Wadsley, "Crystal chemistry of stoichiometric compounds," Revs. Pure and Appl. Chem. **5**, 165–193 (1955).

[47]P. Battle, A. Cheetham, G. Long, and G. Longworth., "A study of the magnetic properties of iron(III) molybdate, by susceptibility, Mössbauer, and neutron diffraction techniques," Inorg. Chem. **21**, 4223–4228 (1982).

[48]F. Portemer, M. Sundberg, L. Kihlborg, and M. Figlarz, "Homologues of Mo_4O_{11}(mon) in the Mo-W-O system prepared by soft chemistry," J. Solid State Chem. **103**, 403–414 (1993).

[49]C. Zhang, M. C. Gao, Y. Yang, and F. Zhang, "Thermodynamic modeling and first-principles calculations of the Mo-O system," CALPHAD **45**, 178–187 (2014).

[50]H.-S. Kim, J. B. Cook, S. H. Tolbert, and B. Dunn, "The development of pseudocapacitive properties in nanosized-MoO_2," J. Electrochem. Soc. **162**, A5083–A5090 (2015).

[51]J. J. Auborn and Y. L. Barberio, "Lithium intercalation cells without metallic lithium," J. Electrochem. Soc. **134**, 638–641 (1987).

[52]Y. Shi, B. Guo, S. A. Corr, Q. Shi, Y.-S. Hu, K. R. Heier, L. Chen, R. Seshadri, and G. D. Stucky, "Ordered mesoporous metallic MoO_2 materials with highly reversible lithium storage capacity," Nano Lett. **9**, 4215–4220 (2009).

[53]X. Ji, P. S. Herle, Y. Rho, and L. F. Nazar, "Carbon/MoO_2 composite based on porous semi-graphitized nanorod assemblies from in situ reaction of tri-block polymers," Chem. Mater. **19**, 374–383 (2007).

[54]L. C. Yang, Q. S. Gao, Y. H. Zhang, Y. Tang, and Y. P. Wu, "Tremella-like molybdenum dioxide consisting of nanosheets as an anode material for lithium ion battery," Electrochem. Commun. **10**, 118–122 (2008).

[55]K. A. See, M. A. Lumley, G. D. Stucky, C. P. Grey, and R. Seshadri, "Reversible capacity of conductive carbon additives at low potentials: Caveats for testing alternative anode materials for Li-ion batteries," J. Electrochem. Soc. **164**, A327–A333 (2017).

[56]A. Manthiram and C. Tsang, "Synthesis of amorphous $MoO_{2+\delta}$ and its electrode performance in lithium batteries," J. Electrochem. Soc. **143**, L143–L145 (1996).

[57]M. Takeuchi, H. Fujimoto, and Y. Kida, "Cycle performance and molybdenum dissolution into electrolyte in MoO_2 anode for lithium secondary batteries," ECS Meet. Abstr. **218**, 1101 (2010).

[58]J. Barker, M. Y. Saidi, and J. L. Swoyer, "Synthesis and electrochemical insertion properties of the layered Li_xMoO_2 phases ($x = 0.74$, 0.85, and 1.00)," Electrochem. Solid-State Lett. **6**, A252–A256 (2003).

[59]L. Campanella and G. Pistoia, "MoO_3: A new electrode material for nonaqueous secondary battery applications," J. Electrochem. Soc. **118**, 1905–1908 (1971).

[60]F. W. Dampier, "The cathodic behavior of CuS, MoO_3, and MnO_2 in lithium cells," J. Electrochem. Soc. **121**, 656–660 (1974).

[61]L. Mai, B. Hu, W. Chen, Y. Qi, C. Lao, R. Yang, Y. Dai, and Z. L. Wang, "Lithiated MoO_3 nanobelts with greatly improved performance for lithium batteries," Adv. Mater. **19**, 3712–3716 (2007).

[62]S.-H. Lee, Y.-H. Kim, R. Deshpande, P. A. Parilla, E. Whitney, D. T. Gillaspie, K. M. Jones, A. H. Mahan, S. Zhang, and A. C. Dillon, "Reversible lithium-ion insertion in molybdenum oxide nanoparticles," Adv. Mater. **20**, 3627–3632 (2008).

[63]J. S. Chen, Y. L. Cheah, S. Madhavi, and X. W. Lou, "Fast synthesis of α-MoO_3 nanorods with controlled aspect ratios and their enhanced lithium storage capabilities," J. Phys. Chem. C **114**, 8675–8678 (2010).

[64]J. O. Besenhard, J. Heydecke, and H. P. Fritz, "Characteristics of molybdenum oxide and chromium oxide cathodes in primary and secondary organic electrolyte lithium batteries. I. morphology, structure, and their changes during discharge and cycling," Solid State Ion. **6**, 215–224 (1982).

[65]V. S. Saji and C.-W. Lee, "Molybdenum, molybdenum oxides and their electrochemistry," ChemSusChem **5**, 1146–1161 (2012).

[66]L. Zhou, L. Yang, P. Yuan, J. Zou, Y. Wu, and C. Yu, "α-MoO_3 nanobelts: A high performance cathode material for lithium ion batteries," J. Phys. Chem. C **114**, 21868–21872 (2010).

[67]T. Brezesinski, J. Wang, S. H. Tolbert, and B. Dunn, "Ordered mesoporous α-MoO_3 with iso-oriented nanocrystalline walls for thin-film pseudocapacitors," Nat. Mater. **9**,

146–151 (2010).

[68]H.-S. Kim, J. B. Cook, H. Lin, J. S. Ko, S. H. Tolbert, V. Ozolins, and B. Dunn, "Oxygen vacancies enhance pseudocapacitive charge storage properties of MoO_{3-x}," Nat. Mater. **16**, 454–460 (2017).

[69]G. Pistoia, C. Temperoni, P. Cignini, M. Icovi, and S. Panero, "Non-stoichiometric molybdenum oxides as cathodes for lithium cells: Part III. cells based on $Mo_{18}O_{52}$," J. Electroanal. Chem. **108**, 169–180 (1980).

[70]P. Fiordiponti, G. Pistoia, C. Temperoni, M. Icovi, and S. Panero, "Non-stoichiometric molybdenum oxides as cathodes for lithium cells: Part IV. factors influencing the performance of Li/Mo_8O_{23} batteries," J. Electroanal. Chem. **108**, 181–190 (1980).

[71]J. O. Besenhard and R. Schöllhorn, "The discharge reaction mechanism of the MoO_3 electrode in organic electrolytes," J. Power Sources **1**, 267–276 (1976/77).

[72]M. Icovi, S. Panero, A. D'Agate, G. Pistoia, and C. Temperoni, "Non-stoichiometric molybdenum oxides as cathodes for lithium cells: Part II. secondary batteries," J. Electroanal. Chem. **102**, 343–349 (1979).

[73]P. Meduri, E. Clark, J. H. Kim, E. Dayalan, G. U. Sumanasekera, and M. K. Sunkara, "MoO_{3-x} nanowire arrays as stable and high-capacity anodes for lithium ion batteries," Nano Lett. **12**, 1784–1788 (2012).

[74]R. H. Sánchez, L. Treviño, A. F. Fuentes, A. Martínez-de la Cruz, and L. M. Torres-Martínez, "Electrochemical lithium insertion in two polymorphs of a reduced molybdenum oxide (γ and γ'-Mo_4O_{11})," J. Solid State Electrochem. **4**, 210–215 (2000).